Inorg. Chem. **2008**, *47*, 10509−10521

Essential Role of the Ancillary Ligand in the Color Tuning of Iridium Tetrazolate Complexes

Stefano Stagni,*,† Silvia Colella,‡,§ Antonio Palazzi,*,† Giovanni Valenti,|| Stefano Zacchini,† Francesco Paolucci,|| Massimo Marcaccio,*,|| Rodrigo Q. Albuquerque,‡ and Luisa De Cola*,‡

Dipartimento di Chimica Fisica ed Inorganica, Università di Bologna, viale Risorgimento 4, I-40136 Bologna, Italy, Dipartimento di Chimica "G. Ciamician", Università di Bologna, via Selmi 2, I-40126 Bologna, Italy, and Physikalisches Institut and Center for Nanotechnology (CeNTech), Westfälische Wilhelms-Universität Münster, Mendelstrasse 7, 48149 Münster, Germany

Received June 24, 2008

We report on the synthesis and physical chemical characterization of a class of heteroleptic mononuclear cyclometalated bis(phenylpyridine)iridium(III) complexes with tetrazolate chelate ligands, such as the deprotonated form of 2-(1*H*-tetrazol-5-yl)pyridine (**PyTzH**), 2-(1*H*-tetrazol-5-yl)pyrazine (**PzTzH**), and 5-bromo-2-(1*H*-tetrazol-5-yl)pyridine (**BrPyTzH**). The electrochemical and photophysical investigations of the resulting iridium(III) complexes revealed a rather wide span of redox and emission properties as a consequence of the nature of the ancillary tetrazolate ligand. In particular, within a series of the three neutral species, the emission observed changes from the blue-green of the pyridyltetrazolate complex to the red of that containing the pyrazinyltetrazolate ligand. The bromo-containing species, despite it displaying poor photophysical performances, is a synthetically attractive building block for the construction of polymetallic architectures. Moreover, the investigation of the reactivity toward electrophiles of one of the neutral mononuclear complexes, by methylation of the coordinated tetrazolate ligand, has also allowed further tuning of the electronic properties. In the latter case, the emission color tuning is also associated with a simple method for the conversion of a neutral species, a potentially triplet emitter for organic light-emitting devices, into the corresponding methylated cation, which might be used as a dopant for light-emitting electrochemical cell type devices or as a marker for biological labeling.

Introduction

Over the past few years, an intense research effort has been devoted to the design of a large number of neutral and cationic cyclometalated iridium(III) complexes.[1] The enormous interest in this particular class of organometallic compounds stems from their outstanding photophysical properties, which have constituted the driving force for their application as photoactive units for light-emitting materials (organic light-emitting devices, OLEDs, and light-emitting electrochemical cells, LEECs)[1,2] as well as sensitizers for solar cells[3] or luminescent probes for biological labeling systems.[4] In general, the properties of phenylpyridine-based iridium(III) derivatives[5] are compared to those of the

* To whom correspondence should be addressed. E-mail: stefano.stagni@unibo.it (S.S.), palazzi@ms.fci.unibo.it (A.P.), massimo.marcaccio@unibo.it (M.M.), decola@uni-muenster.de (L.D.).

† Dipartimento di Chimica Fisica ed Inorganica, Università di Bologna.

‡ Westfälische Wilhelms-Universität Münster.

§ Present address: National Nanotechnology Laboratory of CNR-INFM, via Arnesano, 73100 Lecce, Italy.

|| Dipartimento di Chimica "G. Ciamician", Università di Bologna.

(1) (a) Flamigni, L.; Barbieri, A.; Sabatini, C.; Ventura, B.; Barigelletti, F. *Top. Curr. Chem.* **2007**, *281*, 143, and references cited therein. (b) See also: Dixon, I. M.; Collin, J.-P.; Sauvage, J.-P.; Flamigni, L.; Encinas, S.; Barigelletti, F. *Chem. Soc. Rev.* **2000**, *29*, 385.

(2) (a) Holder, E.; Langeveld, B. M. W.; Schubert, U. S. *Adv. Mater.* **2005**, *17*, 1109, and references cited therein. (b) Baldo, M. A.; Thompson, M. E.; Forrest, S. R. *Nature* **2000**, *403*, 750. (c) Adachi, C.; Baldo, M. A.; Forrest, S. R.; Thompson, M. E. *Appl. Phys. Lett.* **2000**, *77*, 904. (d) Adachi, C.; Baldo, M. A.; Thompson, M. E.; Forrest, S. R. *J. Appl. Phys.* **2001**, *90*, 5048.

(3) (a) Chi, Y.; Chou, P.-T. *Chem. Soc. Rev.* **2007**, *36*, 1421, and references cited therein. See also: (b) Mayo, E. I.; Kilsa, K.; Tirrell, T.; Djurovich, P. I.; Tamayo, A.; Thompson, M. E.; Lewis, N. S.; Gray, H. B. *Photochem. Photobiol. Sci.* **2006**, *5*, 871.

(4) (a) Yu, M.-X.; Zhao, Q.; Shi, L.-X.; Li, F.-Y.; Zhou, Z.-G.; Yang, H.; Yia, T.; Huang, C.-H. *Chem. Commun.* **2008**, 2115. (b) Lo, K. K. W.; Lau, J. S. Y. *Inorg. Chem.* **2007**, *46*, 700. (c) Lo, K. K. W.; Zhang, K. Y.; Chung, C. K.; Kwok, K. Y. *Chem.—Eur. J.* **2007**, *13*, 7110. (d) Lo, K. K.W.; Chung, C. K.; Zhu, N. *Chem.—Eur. J.* **2006**, *12*, 1500, and references cited therein.

10.1021/ic801157k CCC: $40.75
Published on Web 10/22/2008

isoelectronic and structurally analogous ruthenium(II) diimine complexes.[6] Iridium(III) compounds display longer excited-state lifetimes, higher luminescence efficiencies, and, in particular, an emission color tunability that covers almost the entire visible spectrum,[1,7,8] allowing their use for the construction of white light[9] or near-infrared (NIR) emitters.[10] A similar improvement of the photophysical performances is attributed to some key factors, the first of which is represented by the chance of harvesting both singlet and triplet excited states, as a result of the strong spin−orbit coupling effect due to the iridium(III) metal center.[1,5,11] In addition, because the emission of the iridium(III)-cyclometalated complexes is believed to result from excited levels having metal-to-ligand charge transfer (MLCT) character together with significant amounts of ligand-centered (LC) contributions,[1,8e,12] the choice of the appropriate set of cyclometalating (C∧N) or ancillary (L) ligands in the design of homoleptic, $[Ir(C\wedge N)_3]$,[7a,8g,h] or heteroleptic, $[Ir(C\wedge N)_2L]^{n+}$($n = 0, 1$), type complexes,[7b−d,8a−e,13] leads to the spanning of the emission energies over a wide wavelength range. The nature of the third ligand L, for this latter class of compounds, can also determine the charge of the resulting iridium(III) species and, hence, their possible use as emissive dopants for OLEDs (neutral complexes) or for LEECs (charged species).[2] Among the numerous examples reported in the literature, chelating ligands containing five-membered N-heterocycles, such as 2-pyridylpyrazoles,[14] have been frequently used for the synthesis of either homoleptic[8g,h] or heteroleptic[13d,15b] iridium(III) compounds. In this context, other N−H acidic pyridylazoles have been less often considered. Nevertheless, promising results were recently obtained by the use of 1,2,4-triazole-based derivatives for the design of blue-emitting $[Ir(C\wedge N)_2L]$-type complexes,[8a,b,e,f,15b] while only one member of the tetrazole family (RCN_4H), 2-pyridyltetrazole, has been included in the coordination sphere of photophysically interesting iridium(III) species.[15] In the latter case, the tuning of the highest occupied molecular orbital (HOMO)−lowest unoccupied molecular orbital (LUMO) gap of the resulting $[Ir(C\wedge N)_2L]$-type compounds was achieved by the introduction of various electron-withdrawing or electron-donor substituents in the skeleton of the cyclometalating phenylpyridines (C∧N),[15a] leaving the pyridyltetrazolate moiety unaltered. By adopting an opposite strategy, we now discuss the results of the latest development of our research, centered on the coordination chemistry of tetrazolate-based ligands.[16,17] The synthesis, reactivity, and investigation of the electrochemical and photophysical properties of three novel heteroleptic iridium(III) neutral complexes of the general formula $[Ir(C\wedge N)_2(N\wedge N)]$ (see Scheme 1), with the same set of cyclometalating (C∧N) units and different ancillary tetrazolate chelating ligands (N∧N), are herein reported. Impor-

(5) Evans, R. C.; Douglas, P.; Winscom, C. J. *Coord. Chem. Rev.* **2006**, *250*, 2093.

(6) Campagna, S.; Puntoriero, F.; Nastasi, F.; Bergamini, G.; Balzani, V. *Top. Curr. Chem.* **2007**, *280*, 117, and references cited therein.

(7) (a) For red-emitting species, see: Tsuboyama, A.; Iwawaki, H.; Furugori, M.; Mukaide, T.; Kamatani, J.; Igawa, S.; Moriyama, T.; Miura, S.; Takiguchi, T.; Okada, S.; Hoshino, M.; Ueno, K. *J. Am. Chem. Soc.* **2003**, *125*, 12971. (b) Liang, B.; Jiang, C. Y.; Chen, Z.; Zhang, X. J.; Shi, H. H.; Cao, Y. *J. Mater. Chem.* **2006**, *16*, 1281–1286. (c) Liu, Z. W.; Guan, M.; Bian, Z. Q.; Nie, D. B.; Gong, Z. L.; Li, Z. B.; Huang, C. H. *Adv. Funct. Mater.* **2006**, *16*, 1441. (d) Song, Y.-H.; Yeh, S.-J.; Chen, C.-T.; Chi, Y.; Liu, C.-S.; Yu, J.-K.; Hu, Y.-H.; Chou, P.-T.; Peng, S.-M.; Lee, G.-H. *Adv. Funct. Mater.* **2004**, *14*, 1221, and references cited therein.

(8) (a) For blue-emitting species, see: Chang, C.-F.; Cheng, Y.-M.; Chi, Y.; Chiu, Y.-C.; Lin, C.-C.; Lee, G.-H.; Chou, P.-T.; Chen, C.-C.; Chang, C.-H.; Wu, C.-C. *Angew. Chem., Int. Ed.* **2008**, *47*, 4542. (b) Orselli, E.; Kottas, G. S.; Konradsson, A. E.; Coppo, P.; Fröhlich, R.; De Cola, L.; van Dijken, A.; Büchel, M.; Börner, H. *Inorg. Chem.* **2007**, *46*, 11082, and references cited therein. See also: (c) Yang, C. H.; Cheng, Y. M.; Chi, Y.; Hsu, C. J.; Fang, F. C.; Wong, K. T.; Chou, P. T.; Chang, C. H.; Tsai, M. H.; Wu, C. C. *Angew. Chem., Int. Ed.* **2007**, *46*, 2418. (d) Ragni, R.; Plummer, E. A.; Brunner, K.; Hofstraat, J. W.; Babudri, F.; Farinola, G. M.; Naso, F.; De Cola, L. *J. Mater. Chem.* **2006**, *16*, 1161. (e) Yang, C. H.; Li, S. W.; Chi, Y.; Cheng, Y. M.; Yeh, Y. S.; Chou, P. T.; Lee, G. H.; Wang, C. H.; Shu, C. F. *Inorg. Chem.* **2005**, *44*, 7770. (f) Coppo, P.; Plummer, E. A.; De Cola, L. *Chem. Commun.* **2004**, 1774. (g) Sajoto, T.; Djurovich, P. I.; Tamayo, A.; Yousufuddin, M.; Bau, R.; Thompson, M. E.; Holmes, R. J.; Forrest, S. R. *Inorg. Chem.* **2005**, *44*, 7992. (h) Tamayo, A. B.; Alleyne, B. D.; Djurovich, P. I.; Lamansky, S.; Tsyba, I.; Ho, N. N.; Bau, R.; Thompson, M. E. *J. Am. Chem. Soc.* **2003**, *125*, 7377.

(9) (a) Sun, Y. R.; Giebink, N. C.; Kanno, H.; Ma, B. W.; Thompson, M. E.; Forrest, S. R. *Nature* **2006**, *440*, 908, and references cited therein. (b) Kanno, H.; Holmes, R. J.; Sun, Y.; Kena-Cohen, S.; Forrest, S. R. *Adv. Mater.* **2006**, *18*, 339. (c) Coppo, P.; Duati, M.; Kozhevnikov, V. N.; Hofstraat, J. W.; De Cola, L. *Angew. Chem., Int. Ed.* **2005**, *44*, 1806. (d) Gong, X.; Wang, S.; Moses, D.; Bazan, G. C.; Heeger, A. J. *Adv. Mater.* **2005**, *17*, 2053. (e) D'Andrade, B. W.; Forrest, S. R. *Adv. Mater.* **2004**, *16*, 1585.

(10) (a) Mehlstäubl, M.; Kottas, G. S.; Colella, S.; De Cola, L. *Dalton Trans.* **2008**, 2385. (b) Chen, H.-Y.; Yang, C.-H.; Chi, Y.; Cheng, Y.-M.; Yeh, Y.-S.; Chou, P.-T.; Hsieh, H.-Y.; Liu, C.-S.; Peng, S.-M.; Lee, G.-H. *Can. J. Chem.* **2006**, *84*, 309.

(11) Montalti, M.; Credi, A.; Prodi, L.; Gandolfi, M. T. *Handbook of Photochemistry*; Taylor and Francis: Boca Raton, FL, 2006,

(12) (a) Yersin, H. *Top. Curr. Chem.* **2004**, *241*, 1. (b) Lamansky, S.; Djurovich, P.; Murphy, D.; Abdel-Razzaq, F.; Kwong, R.; Tsyba, I.; Bortz, M.; Mui, B.; Bau, R.; Thompson, M. E. *Inorg. Chem.* **2001**, *40*, 1704.

(13) (a) For some recent examples of cationic $[Ir(C\wedge N)_2L]^+$ species, see: Dragonetti, C.; Falciola, L.; Mussini, P.; Righetto, S.; Roberto, D.; Ugo, R.; Valore, A.; De Angelis, F.; Fantacci, S.; Sgamellotti, A.; Ramon, M.; Muccini, M. *Inorg. Chem.* **2007**, *46*, 8533. (b) Nazeeruddin, Md. K.; Wegh, R. T.; Zhou, Z.; Klein, C.; Wang, Q.; De Angelis, F.; Fantacci, S.; Grätzel, M. *Inorg. Chem.* **2006**, *45*, 9245. (c) Zhao, Q.; Liu, S.; Shi, M.; Wang, C.; Yu, M.; Li, L.; Li, F.; Yi, T.; Huang, C. *Inorg. Chem.* **2006**, *45*, 6152. (d) Tamayo, A. B.; Garon, S.; Sajoto, T.; Djurovich, P. I.; Tsyba, I. M.; Bau, R.; Thompson, M. E. *Inorg. Chem.* **2005**, *44*, 8723. (e) Nazeeruddin, Md. K.; Humphry-Baker, R.; Berner, D.; Rivier, S.; Zuppiroli, L.; Grätzel, M. *J. Am. Chem. Soc.* **2003**, *125*, 8790, and references cited therein.

(14) (a) For an excellent overview of the various 2-pyridylazolates employed as ligands for phosphorescent species, see: Chou, P.-T.; Chi, Y. *Chem.—Eur. J.* **2007**, *13*, 380, and references cited therein. See also: (b) Chang, C.-J.; Yang, C.-H.; Chen, K.; Chi, Y.; Shu, C.-F.; Ho, M.-L.; Yeh, Y.-S.; Chou, P.-T. *Dalton Trans.* **2007**, *1881*and references cited therein.

(15) (a) Wu, L.-L.; Yang, C.-H.; Sun, I.-W.; Chu, S.-Y.; Kao, P.-C.; Huang, H.-H. *Organometallics* **2007**, *26*, 2017. (b) Yeh, S.-J.; Wu, M.-F.; Chen, C.-T.; Song, Y.-H.; Chi, Y.; Ho, M.-H.; Hsu, S.-F.; Chen, C. H. *Adv. Mater.* **2005**, *17*, 285.

(16) (a) For polypyridylruthenium(II) tetrazolate complexes, see: Stagni, S.; Orselli, E.; Palazzi, A.; De Cola, L.; Zacchini, S.; Femoni, C.; Marcaccio, M.; Paolucci, F.; Zanarini, S. *Inorg. Chem.* **2007**, *46*, 9126. (b) Stagni, S.; Palazzi, A.; Zacchini, S.; Ballarin, B.; Bruno, C.; Marcaccio, M.; Paolucci, F.; Monari, M.; Carano, M.; Bard, A. J. *Inorg. Chem.* **2006**, *45*, 695. (c) Zanarini, S.; Bard, A. J.; Marcaccio, M.; Palazzi, A.; Paolucci, F.; Stagni, S. *J. Phys. Chem. B* **2006**, *110*, 22551. (d) Duati, M.; Tasca, S.; Lynch, F. C.; Bohlen, H.; Vos, J. G.; Stagni, S.; Ward, M. D. *Inorg. Chem.* **2003**, *42*, 8377. (e) Massi, M.; Cavallini, M.; Stagni, S.; Palazzi, A.; Biscarini, F. *Mater. Sci. Eng. C* **2003**, *23*, 923.

(17) (a) For cyclopentadienyliron(II) tetrazolate complexes, see: Palazzi, A.; Stagni, S. *J. Organomet. Chem.* **2005**, *690*, 2052. (b) Palazzi, A.; Stagni, S.; Monari, M.; Selva, S. *J. Organomet. Chem.* **2003**, *669*, 135. (c) Palazzi, A.; Stagni, S.; Bordoni, S.; Monari, M.; Selva, S. *Organometallics* **2002**, *21*, 3774.

Scheme 1. Schematic Formulas of the Ligands, Complexes, and Acronyms Used in This Paper

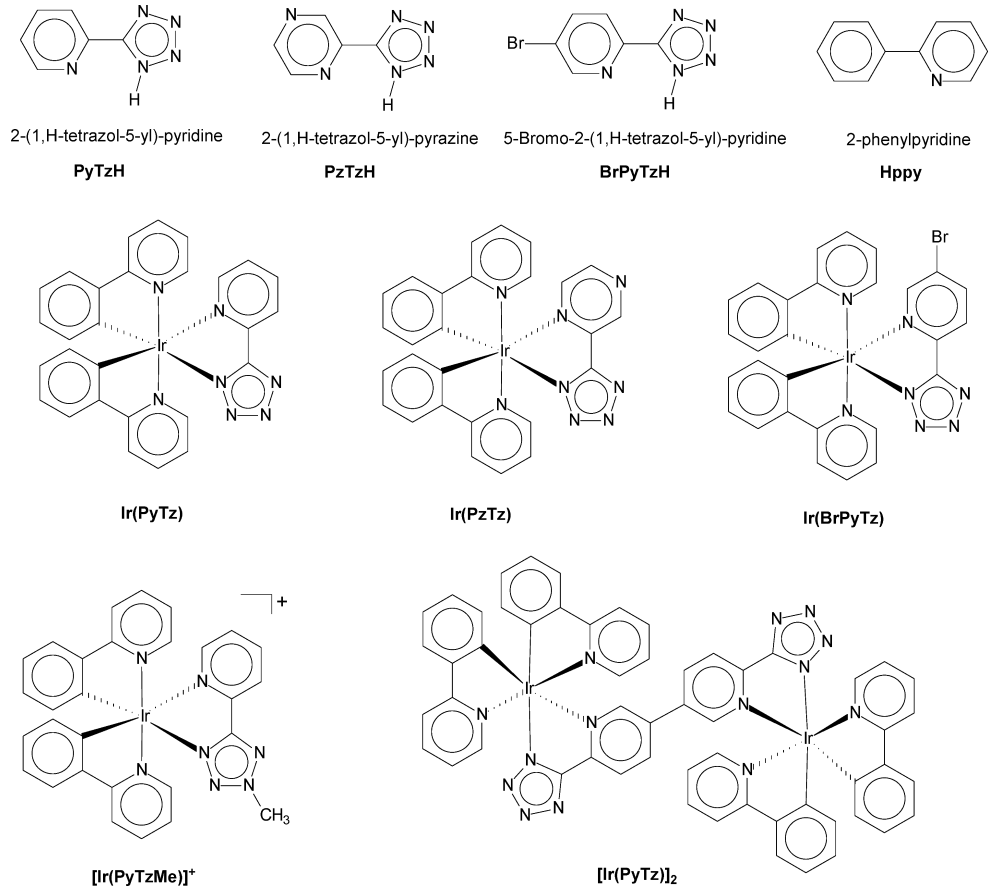

Scheme 2. Synthetic Procedure Adopted for the Formation of the Neutral Species and Atom Labeling

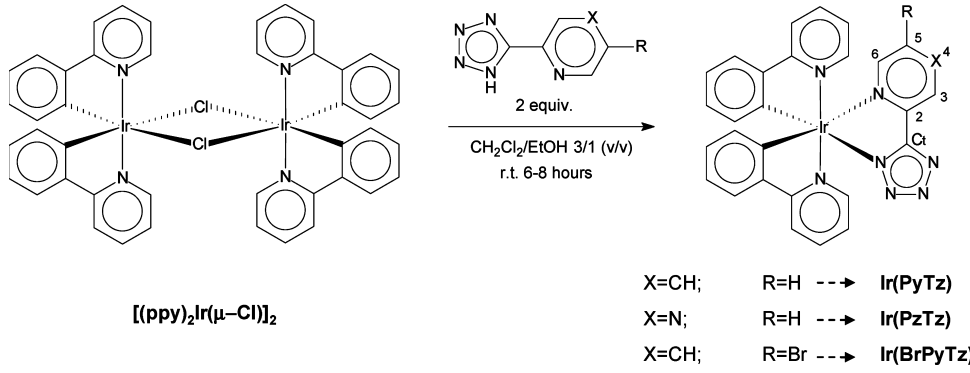

tantly, the great versatility of tetrazoles has been exploited, by taking advantage of the multidentate nature of the tetrazolate ($-CN_4$) moiety, which allows "switching" of the neutral complexes to the corresponding cationic derivatives. Indeed, following a "chemistry on the complex" procedure, the neutral pyridyltetrazolate complex **Ir(PyTz)** has been converted into the cationic **[Ir(PyTzMe)]**$^+$ one by the addition of a methyl group, and it has also been thoroughly characterized.

Results and Discussion

Syntheses, NMR Characterization, and X-ray Diffraction Studies. The synthesis of the target neutral compounds **Ir(PyTz)**, **Ir(PzTz)**, and **Ir(BrPzTz)** (Scheme 2) has been accomplished by following a previously reported procedure[8e] involving the reaction of the dichloro-bridged iridium dimer $[(ppy)_2Ir(\mu\text{-}Cl)]_2$ with a slight excess of the desired tetrazole in a 3:1 (v/v) dichloromethane/ethanol mixture. All complexes were purified by alumina-filled column chromatography, and the confirmation of their composition was provided by electrospray ionization mass spectrometry (ESI-MS).

The NMR characterization of all iridium(III) derivatives (see Table 1) is consistent with the presence of a third unsymmetrical ligand, as shown by each ^1H and ^{13}C NMR spectrum (Figures S1−S7 in the Supporting Information) displaying a number of resonances equal to the total number of protons or carbons of the complex. The distinction of the

Table 1. Selected ^{1}H (600 MHz) and ^{13}C (100 MHz) NMR Data[a] of All of the Ligands and Complexes Reported in This Paper (See Scheme 2 for Atom Labeling)

entry	δC_t	δH_3	δC_3	δH_4	δC_4	δH_5	δC_5	δH_6	δC_6
PyTzH	154.9	8.19	122.7	8.04	138.3	7.59	126.1	8.76	150.1
Ir(PyTz)[a]	163.6	8.34	122.5	8.18	140.0	7.48	126.8	7.68	149.6
[Ir(PyTzMe)]$^+$	167.7	8.40	125.5	8.16	141.3	7.56	130.5	7.90	152.2
[Ir(PyTz)]$_2$[b]	164.3	8.38	122.8	7.91	139.1		126.0	7.87	150.1
PzTzH	153.5	9.37	143.3			8.85	146.8	8.85	144.8
Ir(PzTz)	162.2	9.62	144.6			8.49	147.3	7.78	143.7
BrPyTzH	154.5	8.14	124.2	8.31	140.9		122.6	8.92	151.0
Ir(BrPyTz)	163.5	9.30	123.7	8.07	141.9		121.9	7.82	151.2

[a] Solvents employed: dimethyl sulfoxide-d_6 for all ligands and complex **Ir(PyTz)**; CD_2Cl_2 for all of the remaining species except **[Ir(PyTzMe)]**$^+$, which was analyzed by using CD_3CN. All experiments were performed at room temperature; chemical shifts are expressed in ppm. [b] See Scheme 4 for atom labeling.

tetrazolate signals from those of the inequivalent phenylpyridines was accomplished with the use of ^{1}H gs-COSY, ^{1}H,^{13}C gs-HSQC, and ^{1}H−^{13}C gs-HMQC NMR two-dimensional techniques. The NMR data of the chelating tetrazolates, which are listed in Table 1, are closely similar to those of the previously reported $[Ru(bpy)_2L]^+$-type complexes.[16a] The tetrazole carbon resonating in the range between 162.2 and 164.3 ppm indicates that coordination occurred through the tetrazole N(1) nitrogen. As we reported earlier,[16a] the presence of the C_t signal in such a downfield region is a reflection of the interannular conjugation effect arising from the coplanar arrangement adopted by the aromatic rings of the 5-substituted tetrazolate moiety.

In addition, important details about the coordination geometry of phenylpyridines and tetrazolate ligands can be deduced from the analysis of the X-ray crystal structures of the complexes (Figure 1 and Table 2). In each case, the iridium(III) center adopts a distorted octahedral coordination geometry with *cis*-metalated carbons and *trans*-phenylpyridine nitrogen atoms, as was previously found in other complexes containing analogous cyclometalated C∧N ligands.[18] The Ir−N (N∧N) distances [2.137(15)−2.196(14) Å] are longer than Ir−N (C∧N) [2.033(15)−2.049(5) Å], as was previously found,[7d,13c] because of the trans influence of the metalated carbon atoms. As a consequence of the coordination of pyridyltetrazolate ligands to the metals, the two aromatic rings are almost coplanar.[19] The Ir−N distances with the pyridyltetrazolate ligands are similar to the ones found in similar iridium(III) complexes.[15a] No major differences in the structures and bonding parameters of the three reported complexes, i.e., **Ir(PyTz)**, **Ir(PzTz)**, and **Ir(BrPyTz)**, have been detected.

Methylation Reaction. The reaction of the neutral complex **Ir(PyTz)** with a stoichiometric amount of methyl triflate led to the formation of a cationic compound that was identified as the methylated complex **[Ir(PyTzMe)]**$^+$ (Scheme 3).

The ^{1}H and ^{13}C NMR spectra of this latter species unambiguously indicate the presence of one methyl group, which resonates at 4.42 and 42.7 ppm, respectively (Figures S1−S7 in the Supporting Information). In addition, a single tetrazole carbon (C_t) resonance at 167.7 ppm provides evidence for regioselective methylation at the tetrazolate ring. This signal is significantly downfield shifted with respect to that of the neutral precursor (see Table 1), and according to our previous studies concerning homologue $[Ru(bpy)_2L]^+$ species, we indicate the tetrazole N(3) nitrogen as the specific site at which methylation occurs.[16a] This feature is clearly observable in the X-ray structure of the cationic complex (see Figure 1 and Table 2). The analysis of the X-ray structure of the cationic **[Ir(PyTzMe)]**$^+$ evidences that methylation does not cause any major variation in the geometry and bonding parameters of the complex, compared to the nonmethylated species, as found in analogous ruthenium(II) species with similar ligands.[16a] In particular, the pyrazinyl and tetrazole rings retain their coplanarity [torsion angles N(1)−C(1)−C(2)−N(5) 1.4(7)° and C(3)−C(2)−C(1)−N(4) 1.0(9)°].

Scheme 3. Methylation of **Ir(PyTz)**

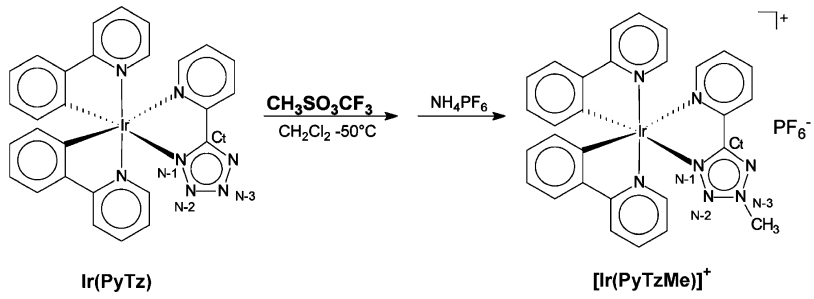

Scheme 4. Homocoupling Reaction of **Ir(BrPyTz)** Species

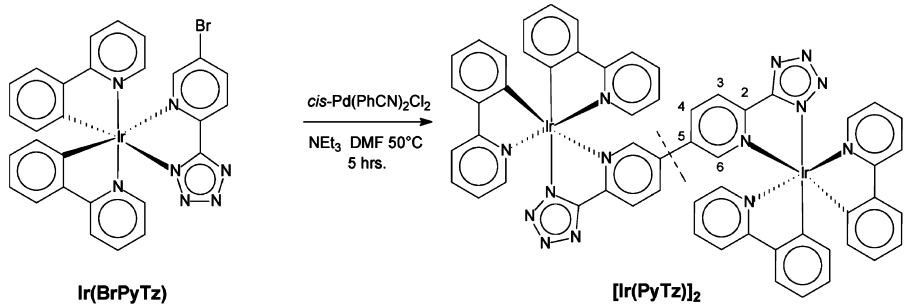

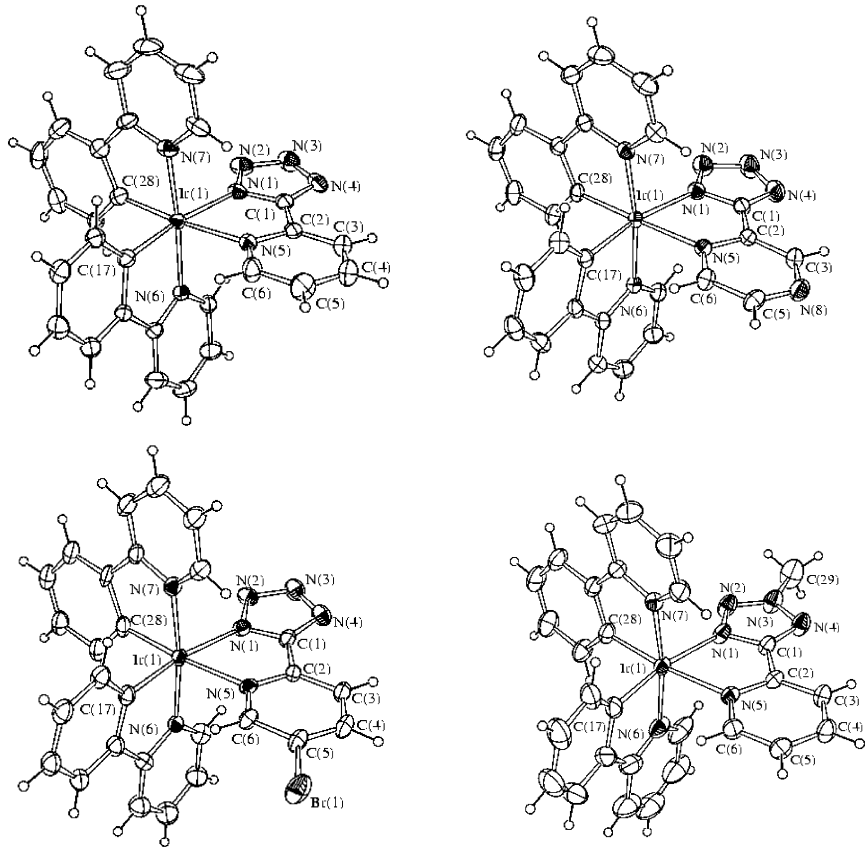

Figure 1. Molecular structures of **Ir(PyTz)** (top, left), **Ir(PzTz)** (top, right), **Ir(BrPyTz)** (bottom, left), and **[Ir(PyTzMe)]**$^+$ (bottom, right), with key atoms labeled. Displacement ellipsoids are at the 30% probability level.

Table 2. Bond Lengths (Å) and Angles (deg) for **Ir(PyTz)**, **Ir(PzTz)**, **Ir(BrPyTz)**, and **[Ir(PyTzMe)]**$^+$

	Ir(PyTz)	**Ir(PzTz)**	**Ir(BrPyTz)**	**[Ir(PyTzMe)]**$^+$
Ir(1)−N(1)	2.140(5)	2.147(3)	2.137(15)	2.143(4)
Ir(1)−N(5)	2.161(5)	2.156(3)	2.196(14)	2.182(4)
Ir(1)−N(6)	2.049(5)	2.041(3)	2.033(15)	2.042(5)
Ir(1)−N(7)	2.047(5)	2.046(3)	2.048(16)	2.048(4)
Ir(1)−C(17)	2.016(6)	2.007(4)	1.987(19)	1.999(5)
Ir(1)−C(28)	2.008(7)	2.002(3)	1.991(19)	2.008(5)
N(1)−N(2)	1.328(7)	1.350(4)	1.34(2)	1.329(6)
N(2)−N(3)	1.313(8)	1.324(5)	1.31(2)	1.301(7)
N(3)−N(4)	1.341(10)	1.343(5)	1.36(3)	1.333(6)
N(4)−C(1)	1.332(8)	1.328(5)	1.31(3)	1.337(7)
C(1)−C(2)	1.438(9)	1.444(5)	1.44(3)	1.460(6)
C(1)−N(1)	1.336(9)	1.340(4)	1.33(2)	1.337(6)
C(5)−Br(1)			1.87(2)	
N(1)−Ir(1)−N(5)	76.8(2)	76.02(11)	75.6(6)	75.57(14)
N(7)−Ir(1)−C(28)	80.2(3)	80.53(14)	80.1(8)	80.24(19)
N(6)−Ir(1)−C(17)	80.6(2)	80.88(13)	79.7(7)	81.3(3)
Ni(1)−Ir(1)−C(17)	171.5(3)	168.73(13)	170.0(7)	168.73(17)
N(5)−Ir(1)−C(28)	174.5(3)	178.14(13)	174.8(7)	173.20(17)
N(6)−Ir(1)−N(7)	175.0(2)	171.93(11)	172.9(6)	171.97(17)

Redox Behavior. The electrochemistry of the mononuclear complexes was investigated in an acetonitrile (ACN) solution by cyclic voltammetry at room temperature. The potentials of the various processes are collected in Table 3.

In the region of the positive potentials, all of the complexes exhibited a single one-electron reversible process. As was previously reported[13a−c] and also shown by density functional theory (DFT) calculations (vide infra), the oxidation of this class of iridium(III) species can be attributed to the metal center, with a substantial contribution from the ligands. Conversely, the reduction processes are mainly centered on the ligands.

Table 3. Half-Wave ($E_{1/2}$) Redox Potentials[a] (vs SCE) of All Complexes at 25 °C

	$E_{1/2}$/V			
species	oxidation	reduction		
[Ir(PyTz)]	1.13	−2.00		
[Ir(PyTzMe)]$^+$	1.32	−1.56	−2.20	
[Ir(PzTz)]	1.19	−1.47	−2.28	−2.38
[Ir(BrPyTz)]	1.16	−1.73[b]	−2.00	

[a] In a 0.07 M TBAH/ACN solution. [b] Irreversible process; cathodic peak potential.

The oxidation of the three neutral complexes **Ir(PyTz)**, **Ir(PzTz)**, and **Ir(BrPyTz)**, whose cyclic voltammetric (CV) curves are reported in parts a, c, and d of Figure 2, respectively, shows a single reversible one-electron process, within the potential window explored. The corresponding oxidation processes occur at about the same potential, which fall around 1.15 V (see Table 3), indicating that the molecular orbital involved in each complex does not span over the tetrazolate ligand, and this is in agreement with the theoretical data. Despite the small differences in the oxidation potentials, as expected, the oxidation of the pyrazinyltetrazolate complex **Ir(PzTz)** is found to occur at more positive potentials than the homologue pyridyl-based **Ir(PyTz)**. This can be at-

(18) Neve, F.; La Deda, M.; Crispini, A.; Bellusei, A.; Puntoriero, F.; Campagna, S. *Organometallics* **2004**, *23*, 5856.

(19) Torsion angles N(1)−C(1)−C(2)−N(5) are 3.0(9)°, −0.1(5)°, and 9(2)° and C(3)−C(2)−C(1)−N(4) are 4.1(12)°, 0.6(7)°, and 6(3)° for **Ir(PyTz)**, **Ir(PzTz)**, and **Ir(BrPyTz)**, respectively.

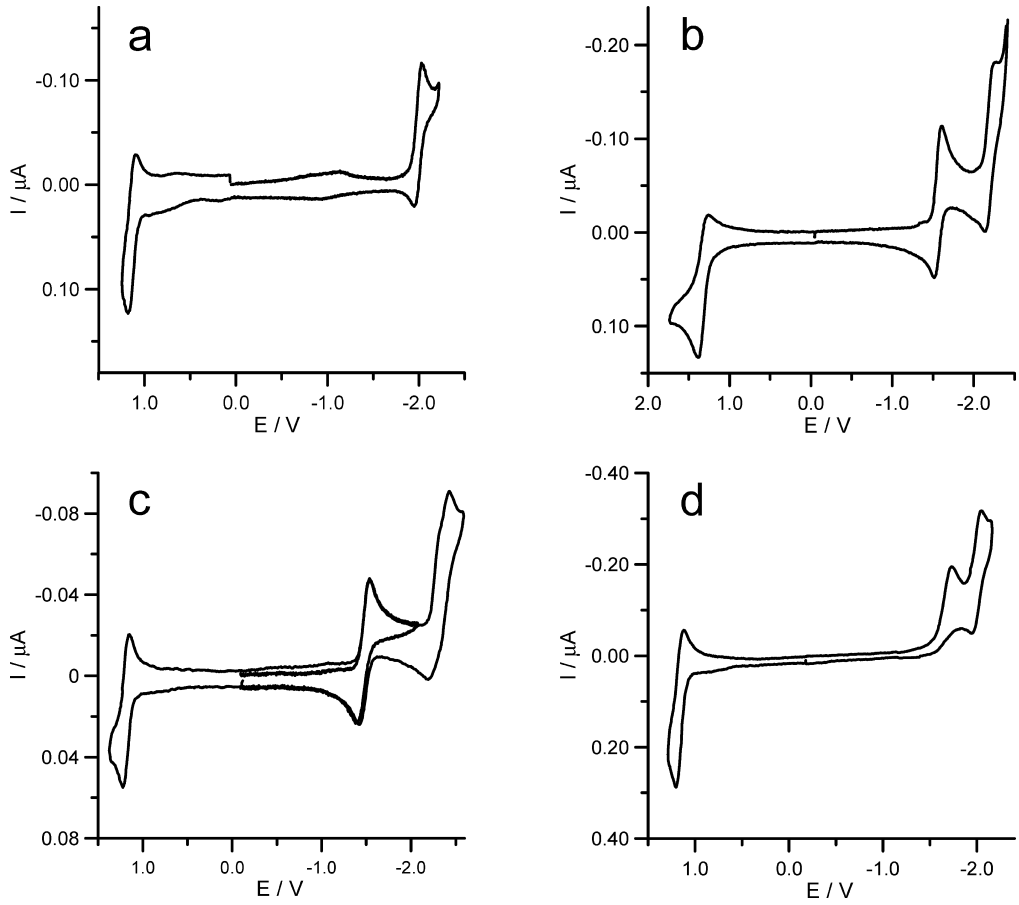

Figure 2. CV curves of 1 mM samples of complexes (a) **Ir(PyTz)**, (b) **[Ir(PyTzMe)]**$^+$, (c) **Ir(PzTz)**, and (d) **Ir(BrPyTz)** in a 0.07 M TBAH/ACN solution; working electrode Pt disk, 125 μm diameter; $T = 25$ °C; scan rate 1 V/s.

tributed to the enhanced electron-withdrawing character of the pyrazine ring of the **PzTz** moiety, which turns into the weaker σ-donor and stronger π-acceptor properties, compared to those of the pyridine ligand. Furthermore, as shown in Figure 2b, the methylation of the tetrazolate ligand (i.e., **[Ir(PyTzMe)]**$^+$ species) moves the oxidation process 190 mV toward more positive potentials. On the basis of the redox behavior and the electronic structure of the analogue ruthenium(II) tetrazolate containing complexes,[16a] such a positive shift value can be mostly accounted for by the increased charge of the methylated complex rather than by the perturbation of the electronic properties of the pyridyltetrazolate ligand itself. In fact, if the molecular orbital involved in the oxidation were largely delocalized over the tetrazole ligand, a higher potential shift would be expected. Thus, all of this evidence supports the small involvement of the tetrazolate ligands in the oxidation process of the iridium complexes investigated herein.

Concerning the reductions, the CV investigation has been carried out by exploring the first processes, in particular those occurring within the potential window down to about −2.5 V. The species **Ir(PyTz)** shows only a one-electron reversible voltammetric wave (Figure 2a) at −2.00 V. The replacement of the 2-pyridyltetrazolate (**PyTz**) ligand with the pyrazinyl homologue in the iridium complex (i.e., **Ir(PzTz)** species) leaves the oxidation (vide supra) practically unchanged, while on the negative potential side, there is a more dramatic effect. Figure 2c shows the CV curve of the **Ir(PzTz)** complex, recorded at room temperature and 1 V/s. It is comprised of two reduction voltammetric waves: the first is a Nernstian one-electron process, while the second one is made up of two closely spaced one-electron reversible reductions. The better electron π-acceptor properties of the 2-pyrazinyltetrazolate ligand, with respect to **PyTz**, makes the first reduction 530 mV easier and, thus, two further processes become accessible within the useful potential window.

On the basis of the electronic properties of the uncoordinated ligands and the comparison of the CV curves of the two complexes **Ir(PyTz)** and **Ir(PzTz)**, the first reduction occurring in **Ir(PzTz)** can be confidently assigned to the tetrazolate ligand, as is also supported by DFT calculations (vide infra). The two further reductions of the species **Ir(PzTz)** are therefore mainly localized on the two phenylpyridyl ligands. Further support to such an assignment comes from the analysis of the reduction processes of the **[Ir(PyTzMe)]**$^+$ compound. As reported in Figure 2b, it shows two reversible one-electron reductions: the first one at −1.56 V and the second at −2.20 V, i.e., at potentials very close to those of the first and second reductions of **Ir(PzTz)**. It is worth noting that replacement of the ligand **PyTz** with **PzTz** is more effective than tetrazole methylation in stabilizing the molecular orbital centered on the tetrazolate ligands. In fact, the first reduction of the species **Ir(PzTz)** is 90 mV easier than that of the complex **[Ir(PyTzMe)]**$^+$. On the

contrary, the second reduction of the methylated species is 80 mV less negative than the corresponding process of **Ir(PzTz)**, as was the presumable consequence of a charge effect.

Finally, concerning the reduction processes of the species **[Ir(BrPyTz)]**, the CV curve, in Figure 2d, shows two one-electron voltammetric waves. The first process remains completely irreversible even at relatively high sweep rates (up to 100 V/s), while the second one is a Nernstian electron transfer. On the basis of the reduction behavior of the aromatic halogen species[20] and the fact that the first reduction is localized on the tetrazolate ligand, the nature of the irreversibility of the process can be confidently attributed to the electron-induced outgoing of the anion Br^- from the ligand **BrPyTz**. Moreover, it is important to note that the second reduction occurs at the same potential as the first one of the species **Ir(PyTz)**, with the last one being the product of the reaction following up the first reduction.[21] These considerations altogether support an electrochemical−chemical−electrochemical (ECE) step mechanism for the reduction of the **Ir(BrPyTz)** complex.

Electronic and Excited-State Properties. The absorption spectra of all complexes were measured at room temperature in dichloromethane solutions and are reported in Table 4 and Figure 3. In each spectrum, the UV region displays the LC $^1\pi \rightarrow \pi^*$ type transitions as the most intense absorption bands. The shoulders appearing in the range between 350 and 450 nm are likely due to CT transitions, with their nature being both spin-allowed (singlet-to-singlet MLCT, ^{1}MLCT) and spin-forbidden (singlet-to-triplet MLCT, ^{3}MLCT). The relatively high intensity of these latter bands reflects the strong spin−orbit coupling effect, which arises from the presence of a third-row transition metal in a high oxidation state such as iridium(III).

All of the new complexes are luminescent at room temperature in a dichloromethane solution, with emission maxima falling in the wavelength range between 480 and 600 nm (Figure 4; see also Figures S8−S11 in the Supporting Information). In particular, among the series represented by the three neutral compounds **Ir(PyTz)**, **Ir(PzTz)**, and **Ir(BrPyTz)**, the photoluminescence spectra of the complex **Ir(PyTz)** and the bromo derivative **Ir(BrPyTz)** display vibronic-structured emission bands. According to the published works concerning analogous iridium(III) cyclometalates,[1,7a,8b] the occurrence of a similar emission shape is attributed to the presence of an excited state resulting from the mixing of comparable percentages of ^{3}LC and ^{3}MLCT states, as was also confirmed by the DFT calculations (vide infra). On the other hand, the pyrazinyl complex **Ir(PzTz)** displays a structureless emission centered at ca. 600 nm, the shape of which is consistent with the prevalent ^{3}MLCT character of the excited state. A similar behavior might be explained by considering that the replacement of a pyridyl ring with the more electron-withdrawing pyrazinyl moiety is

Table 4. Absorption and Emission Spectral Data of All of the Complexes[a]

complex	absorption[b]	emission, 298 K[c,d]							emission, 77 K[c,f]	
	λ_{max} (nm); $10^{-4}\varepsilon$ (M^{-1} cm^{-1})	λ (nm)	τ (μs),[e] dear	τ (μs),[e] air	Φ dear	Φ air	k_r (10^5 s^{-1})	k_{nr} (10^6 s^{-1})	λ (nm), 77 K	τ (μs),[e] 77 K
Ir(PyTz)	259 (4.02), 271 (sh, 3.70), 340 (0.75), 387 (0.45), 417 (sh, 0.30)	481, 510	0.553	0.093	0.143	0.026	2.6	1.5	478	3.69
Ir(PzTz)	256 (4.02), 268 (sh, 3.77), 295 (sh, 2.40), 337 (1.04), 383 (sh, 0.55), 412 (0.37), 460 (sh, 0.09)	601	0.255	0.120	0.090	0.043	3.5	3.6	572	5.66
Ir(BrPyTz)	258 (4.38), 271 (sh, 4.00), 305 (sh, 1.93), 388 (0.46), 417 (sh, 0.35)	482, 511	0.064 (70), 0.389 (30)	0.089 (30), 0.034 (70)	0.017	0.010	1.05	6.1	487	2.6 (36), 4.55 (64)
[Ir(PyTzMe)]$^+$	256 (sh, 2.94), 264 (3.00), 307 (sh, 1.18), 349 (0.44), 377 (0.34), 404 (sh, 0.27)	558	0.516	0.115	0.240	0.012	4.7	1.5	508	4.39

[a] All data for complexes in CH_2Cl_2. [b] "sh" denotes a shoulder. [c] λ_{exc} = 400 nm. [d] Quantum yields are measured versus quinine bisulfate in 1 N H_2SO_4 (λ_{exc} = 350 nm). [e] For the biexponential excited-state lifetimes (τ), the relative weights of the exponential curves are reported in parentheses. [f] In butyronitrile glass.

(20) (a) Benassi, R.; Bertarini, C.; Taddei, F. *Chem. Phys. Lett.* **1996**, *257*, 633. (b) Prasad, M. A.; Sangaranarayanan, M. V. *Chem. Phys. Lett.* **2005**, *414*, 55. (c) Antonello, S.; Maran, F. *Chem. Soc. Rev.* **2005**, *34*, 418. (d) Costentin, C.; Robert, M.; Saveant, J.-M. *Chem. Phys.* **2006**, *324*, 40, and references cited therein.

(21) Further electrochemical investigations are currently underway, and the results will be reported in a following paper.

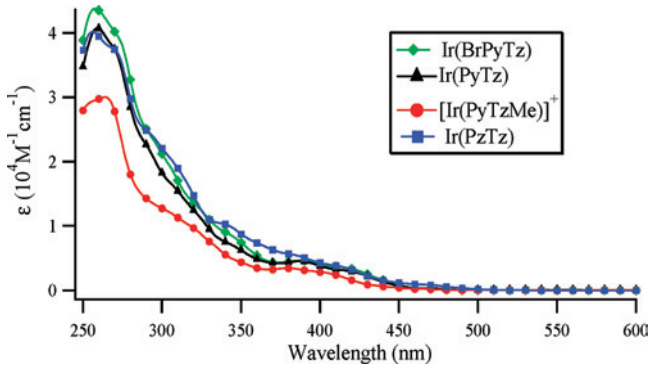

Figure 3. Absorption spectra of all of the species studied in the present paper.

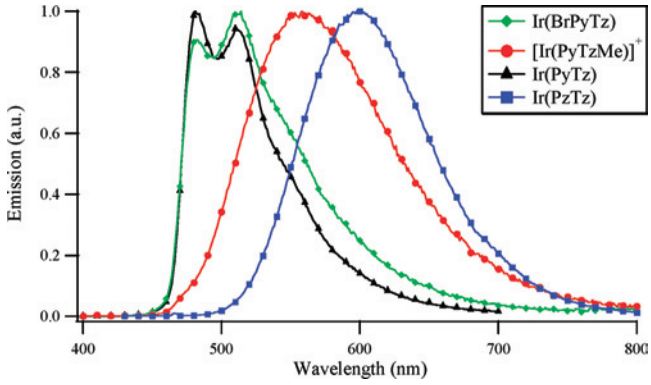

Figure 4. Normalized emission spectra of all of the complexes.

likely responsible for the enhancement of the ^{3}LC−^{3}MLCT energy gap, leading to an emission with prevalent ^{3}MLCT character.

Further support is provided by analysis of the emission spectra recorded at 77 K and in a poly(methyl methacrylate) (PMMA) matrix (Figures S8−S11 in the Supporting Information), which show an appreciable rigidochromic blue shift only in the case of the pyrazinyl complex **Ir(PzTz)**, while the emission profiles of the remaining compounds are substantially unchanged. In a degassed dichloromethane solution, the three neutral complexes reported here show emission quantum yields (Φ) ranging from 14.3%, as in the case of **Ir(PyTz)**, to less than 2% for the bromo-substituted derivative **Ir(BrPyTz)**. In addition, the appreciable decrease of the quantum yield values, which is observed in air-equilibrated solutions, provides confirmation of the triplet character of the emissions. Concerning the radiative lifetimes, the experimental data measured in oxygen-free conditions vary from 0.553 to 0.255 μs and follow the same trend as that observed for the quantum yield values. The radiative lifetime decays were found to be monoexponential for the neutral species **Ir(PyTz)** and **Ir(PzTz)** and for the cationic complex **[Ir(PyTz-Me)]**$^+$, while a biexponential decay was observed for the bromo-substituted complex **Ir(BrPyTz)**. Interestingly, the photochemical behavior of the latter compound, the complex **Ir(BrPyTz)**, might be rationalized by the occurrence of photodegradation processes, consisting of a loss of a bromine atom, upon irradiation at about 400 nm, even though the presence of impurities contaminating the samples could be partially responsible for the extremely low quantum yield. An indirect support to such a photodissociation of the bromine moiety is the very similar mechanism involved in the electrochemical behavior, as discussed above. In addition, the mild conditions that are required for the palladium(0)-mediated homocoupling reaction of complex **Ir(BrPyTz)** (see Scheme 4) provide clear evidence for the presence of a highly reactive C−Br moiety.

This compound was almost completely converted into the corresponding dinuclear complex **[Ir(PyTz)]$_2$** (Figures S6 and S7 in the Supporting Information). The electrochemical and photophysical behavior of this latter symmetrical species is currently under investigation and will be reported in due time. It is worth noting that this latter reaction might represent a further example of the synthetically attractive procedure,[22] in which the bromine-substituted derivative **Ir(BrPyTz)** represents a useful building block for the construction of bi- or polymetallic architectures. The emission performances of each compound were also studied by calculating the radiative (k_r) and nonradiative (k_{nr}) rate constants, which are defined as the ϕ/τ and $(1-\phi)/\tau$ ratios, respectively. Among the series of three neutral complexes, the calculated k_r values span over a narrow range [$(1.0-3.5) \times 10^5$ s^{-1}] and are similar to those of highly luminescent iridium(III) complexes described in previous reports.[8b,13a,b] The nonradiative contants (k_{nr}) are found to be 1 order of magnitude greater than the k_r rates and, probably, represent the main factor for regulating the luminescence behavior of the complexes. Accordingly, the lowest k_{nr} value is displayed by complex **Ir(PyTz)**, which is also the neutral species, showing the highest quantum yield and the longest emission lifetime, among the series. As expected, the photophysical features of the cationic species **[Ir(PyTzMe)]**$^+$ are rather different from those of its neutral precursor **Ir(PyTz)**. Indeed, the photoluminescence spectrum of the methylated compound **[Ir(PyTzMe)]**$^+$, recorded in a dichloromethane solution, displays a broad and structureless emission profile centered at ca. 560 nm. The blue-shifted emission, which is obtained at 77 K and in a PMMA matrix, suggests the prevalent ^{3}MLCT character of the excited state, even though contributions from two distinct levels are observed in the solid-state spectra. As was previously documented for similar species,[8b,22] the occurrence of such an additional structure, which might indicate some ^{3}LC contribution, could be explained in terms of the suppression of the nonradiative decays determined by the rigidochromic effect and by considering that, on going to higher emission energies, the mixing of ^{3}LC and ^{3}MLCT states becomes greater. Among the complexes studied here, the cationic species shows the highest quantum yield (24%) and almost the longest emission lifetime (516 ns), with these values being comparable to those of similar cationic iridium(III) cyclometalates.[13a,b] Also in this case, the calculation of k_r and k_{nr} constants indicates that the emission performances are significantly influenced by nonradiative processes.

DFT Calculations. The geometries of the ground states of the four complexes were optimized by means of DFT calculations, followed by time-dependent DFT (TD-DFT) for calculation of the excited states. The optimized geometries,

(22) Plummer, E. A.; Hofstraat, J. W.; De Cola, L. *Dalton Trans.* **2003**, 2080.

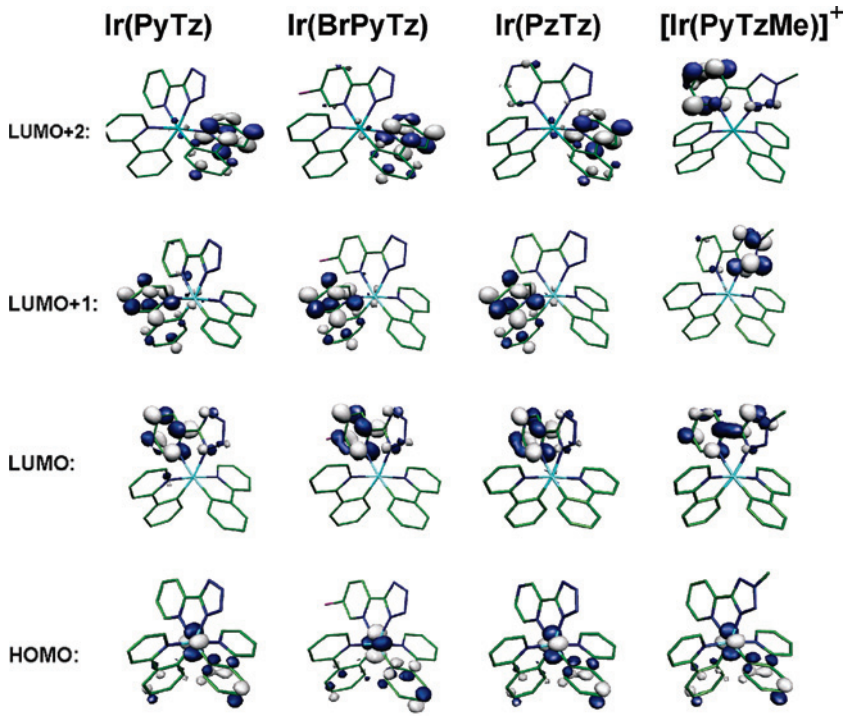

Figure 5. Plots of the molecular orbitals involved in the transition from the lowest triplet states of complexes 1−4 obtained from DFT calculations. The hydrogen atoms are omitted for clarity.

Table 5. Calculated Energies of the Frontier Molecular Orbitals of the Iridium Complexes Investigated

	HOMO/eV	LUMO/eV	LUMO+1/eV
Ir(PyTz)	−5.29	−1.79	−1.68
Ir(BrPyTz)	−5.34	−2.06	−1.74
Ir(PzTz)	−5.43	−2.40	−1.82
[Ir(PyTzMe)]$^+$	−7.80	−5.09	−4.71

Table 6. TD-DFT Calculated Lowest Excited Triplet States and Character of the Transitions for the Four Complexes

complex	λ/nm orbitals involved	nature of the lowest excited state[a,b]
Ir(PyTz)	476 nm	^{3}MLCT + ^{3}LLCT + ^{3}LC
	HOMO ⇒ LUMO+1 (73%)	
	HOMO ⇒ LUMO (10%)	
Ir(BrPyTz)	484 nm	^{3}MLCT + ^{3}LLCT
	HOMO ⇒ LUMO (98%)	
Ir(PzTz)	539 nm	^{3}MLCT + ^{3}LLCT
	HOMO ⇒ LUMO (98%)	
[Ir(PyTzMe)]$^+$	609 nm	^{3}MLCT + ^{3}LLCT
	HOMO ⇒ LUMO (93%)	

[a] The LC states involve the phenylpyridine ligand, while in the LLCT states, the charge is transferred from the phenylpyridine to the tetrazole ligand. [b] The emission energy has been estimated from the absorption transitions.

together with the relevant molecular orbitals showing the highest contribution to the formation of the emitting triplet excited state of complexes **Ir(PyTz)**, **Ir(BrPyTz)**, **Ir(PzTz)**, and **[Ir(PyTzMe)]$^+$**, are plotted in Figure 5.

The calculated structures are in excellent agreement with the crystallographic data and, along with the orbital description, accurately depict the ground-state structures of these complexes. A selection of calculated bond lengths and angles for the ground-state-optimized geometry are given in Table 5. A comparison with the X-ray data (see Table S1 in the Supporting Information) shows that the differences in bond lengths are on the order of a few picometers. The HOMO and LUMO values for **[Ir(PyTzMe)]$^+$** are much lower than those of the other species; this is attributed to the positive charge exhibited only by this complex. As was recently reported, the HOMO energies of cyclometalated iridium(III) complexes[13a,b] with pendant fluorenyl substituents[23] have been calculated to be about −8 eV, which is on the same order of magnitude as that for the cationic species **[Ir(PyTzMe)]$^+$**. The main localization of the frontier molecular orbitals, shown in Figure 5, as well as the relative energies are in tight agreement with the electrochemical and photophysical data. For all of the species, the HOMO is centered on the metal with a substantial contribution from the phenylpyridyl ligands. The LUMO is mainly localized on the tetrazolate ligand. The further two unoccupied molecular orbitals (i.e., LUMO+1 and LUMO+2) are centered on the two phenylpyridines, except for **[Ir(PyTzMe)]$^+$**. However, as for the methylated complex, this is only apparently in contradiction with the electrochemical behavior discussed above. In fact, the molecular orbital description of the fully optimized one-electron-reduced methylated species, that is, **[Ir(PyTzMe)]**, shows that the LUMO (which is the LUMO+1 of **[Ir(PyTzMe)]$^+$**) is localized on the phenylpyridine, as well as the successive unoccupied molecular orbital, as shown in Figure S12 in the Supporting Information.

The calculated energies of the lowest triplet states of all of the mononuclear complexes are shown in Table 6. For complexes **Ir(PzTz)**, **Ir(BrPyTz)**, and **[Ir(PyTzMe)]$^+$**, the emitting state arises from HOMO ⇒ LUMO excitations, while in the case of complex **Ir(PyTz)**, it mainly arises from HOMO ⇒ LUMO+1 excitations for symmetry reasons. The calculated emission of complex **Ir(PyTz)** is 476 nm, which

(23) Zeng, X. M.; Tavasli, M.; Perepichka, I. F.; Batsanov, A. S.; Bryce, M. R.; Chiang, C.-J.; Rothe, C.; Monkman, A. P. *Chem.—Eur. J.* **2008**, *14*, 933.

is in excellent agreement with the calculated value (480 nm), as well as for complex **[Ir(BrPyTz)]**, where the values are 484 nm (calcd) and 482 nm (exptl). For **Ir(PzTz)**, the calculated energy of the lowest triplet state is 539 nm, which is considerably lower than the experimental value of 601 nm. A similar discrepancy exists for **[Ir(PyTzMe)]**$^+$, with values 609 nm (calcd) and 558 nm (exptl).[24] In all cases, the excitation from the HOMO greatly decreases the charge density in the iridium center and increases in the ligands, indicating that the emissions of all of the complexes have a very strong MLCT character. Some ligand-to-ligand CT (LLCT) character for the lowest triplet state, as well as a very small LC contribution for the **Ir(PyTz)** species, is also observed.

In all of the complexes, except **Ir(PyTz)**, the triplet appears to be predominantly localized in the tetrazolate chelate ligand and it accounts for the strong variation of the emission energies, which is observed among this series of iridium(III) complexes upon modification of the tetrazolate ligand. In particular, the emitting triplet state resides prevalently on the pyridyl ring of the tetrazolate ligand in the case of complexes **Ir(BrPyTz)** and **Ir(PzTz)**, while it is more delocalized over the whole pyridinetetrazolate ligand for the cation **[Ir(PyTzMe)]**$^+$. This latter feature may explain the high value of the calculated emission wavelength ($\lambda_{calcd} = 609$ nm), which is red-shifted with respect to the other complexes.

At this level of theoretical calculations and also on the basis of the electrochemical data, we cannot exclude the important role of the tetrazolate ligand in the excited state of **Ir(PyTz)** (10% contribution; see Table 6), which can also be expected considering the small energy difference between LUMO and LUMO+1 ($\Delta E_{LUMO+1-LUMO} = 0.11$ eV). Besides, the TD-DFT calculation predicts two further triplet excited states at slightly higher energies, 462 and 453 nm, which involve a larger contribution from the **PyTz** ligand. Anyway, in order to verify the "nonmarginal" role played by **PyTz** in the emitting state of the complex **Ir(PyTz)**, further theoretical studies must be undertaken.

Conclusions

The advantages arising from the incorporation of tetrazolate-based derivatives as chelating ligands in the structure of cyclometalated iridium(III) compounds are represented by the relatively simple methods required for the ligand syntheses and, importantly, by the great photophysical versatility of the resulting iridium(III) complexes. Indeed, within a series of three neutral iridium(III) species, differing only by the nature of the third ancillary tetrazolate ligand, a consistent bathochromic shift of the emission energy is observed on going from a blue-green emitter such as the pyridyltetrazolate complex **Ir(PyTz)** to the red-emitting species represented by its pyrazinyl analogue **Ir(PzTz)**. The electrochemical studies and the DFT calculations performed on these complexes indicate that tuning of the emission energy over more than 100 nm is rationalized with variation of the nature of the tetrazolate ligand. The bromo-substituted complex **Ir(BrPyTz)** deserves a separate comment. Despite its poor photophysical performances, this complex might be an appealing building block for the assembly of polymetallic species by cross-coupling procedures. Finally, the chance of performing electrophilic additions onto tetrazolate complexes represents an important "added value" resulting from the use of these particular ligands. Indeed, the neutral iridium(III) complex **Ir(PyTz)** can be chemo- and regioselectively converted into the cationic methylated species **Ir(PyTzMe)**. This transformation allows the modulation of the photophysical features of the starting neutral species and introduces also the possibility of using these iridium(III) compounds either as neutral emitters for OLEDs or, in the case of charged species, as cationic emitting dopants for LEEC-type devices or markers for biochemical applications.

Experimental Section

Materials. Solvents were dried and distilled under nitrogen prior to use. Unless otherwise stated, chemicals were obtained commercially (e.g., Aldrich) and used without any further purification. The chloro-bridged iridium precursor, $[(ppy)_2Ir(\mu\text{-}Cl)]_2$, was prepared according to the procedure of Watts and co-workers.[25] Flame-dried glassware was employed for all reactions, which were carried out under an argon atmosphere by adopting Schlenk-lines techniques. Throughout this paper, the percentage yields of the product complexes are with reference to the molar quantity of the starting iridium(III) dimer, $[(ppy)_2Ir(\mu\text{-}Cl)]_2$. The atom numbering used for the description of the NMR spectra (see below) is always with reference to Scheme 2.

Warning! *Nitrogen-rich compounds such as tetrazole derivatives and their salts are used as components for explosive mixtures.*[26] *In this laboratory, the reactions described here were run on only a few grams scale and no problems were encountered. However, great caution should be exercised when handling or heating compounds of this type.*

Instrumentation and Procedures. All of the obtained complexes were characterized by elemental analysis and spectroscopic methods. Elemental analyses were performed on a ThermoQuest Flash 1112 series EA instrument. Mass spectra were performed on a Waters ZQ-4000 instrument [ESI-MS; acetonitrile (ACN) was used as the solvent] or on a Thermo Finnigan MAT 95 XP apparatus (electron impact mass spectrometry, EI-MS). The routine NMR spectra (^{1}H and ^{13}C) were always recorded using a Varian Mercury Plus 400 instrument (^{1}H, 400.1 MHz; ^{13}C, 100.0 MHz) or a Varian Inova 600 MHz instrument (^{1}H, 600.0 MHz; ^{13}C, 150.8 MHz). The spectra were referenced internally to a residual solvent resonance and were recorded at 298 K for characterization purposes. Bidimensional ^{1}H$-^{13}$C correlation spectra were measured via gs-HSQC and gs-HMBC experiments,[27] whereas ^{1}H$-^1$H correlations were determined by gs-COSY experiments.[28]

(24) Among the complexes studied in this work, the larger discrepancy between the calculated data and the experimental ones observed for the species **Ir(PzTz)** and **[Ir(PyTzMe)]**$^+$ might be due to not taking into account the solvation effects in the DFT calculations. This is a critical issue, especially when the systems investigated display radiative processes characterized by a predominant ^{3}MLCT nature, as witnessed by the emission profiles reported in Figures S9 and S11 in the Supporting Information.

(25) Sprouse, S.; King, K. A.; Spellane, P. J.; Watts, R. J. *J. Am. Chem. Soc.* **1984**, *106*, 6647.
(26) Butler, R. N. Tetrazoles. In *Comprehensive Heterocyclic Chemistry II*; Storr, R. C., Ed.; Pergamon Press: Oxford, U.K., 1996; Vol. *4*, pp 621−678, and references cited therein.
(27) Wilker, W.; Leibfritz, D.; Kerssebaum, R.; Beimel, W. *Magn. Reson. Chem.* **1993**, *31*, 287.
(28) Hurd, R. E. *J. Magn. Reson.* **1990**, *87*, 422.

Electrochemistry. Tetrabutylammonium hexafluorophosphate (TBAH, from Fluka), as the supporting electrolyte, was used as received. Dry ACN was successively refluxed over, and distilled from, CaH_2 and activated alumina super I neutral (ICN Biomedicals), and it was stored in a specially designed Schlenk flask over 3 Å activated molecular sieves, protected from light.[29] Shortly before the experiment was performed, the solvent was distilled via a closed system into an electrochemical cell containing the supporting electrolyte and the species under examination. Electrochemical experiments were carried out in an airtight single-compartment cell described elsewhere[30] by using platinum as working and counter electrodes and a silver spiral as a quasi-reference electrode. The cell containing the supporting electrolyte and the electroactive compound was dried under vacuum at about 110 °C for at least 60 h before each experiment. All of the $E_{1/2}$ potentials have been directly obtained from CV curves as averages of the cathodic and anodic peak potentials for one-electron peaks and by digital simulation for those processes closely spaced in multielectron voltammetric peaks. The $E_{1/2}$ values are with reference to an aqueous saturated calomel electrode (SCE) and have been determined by adding, at the end of each experiment, ferrocene as an internal standard and measuring them with respect to the ferrocinium/ferrocene couple standard potential. Voltammograms were recorded with a custom-made fast potentiostat[31] controlled by an AMEL model 568 programmable function generator. The potentiostat was interfaced to a Nicolet model 3091 digital oscilloscope, and the data were transferred to a personal computer by the program *Antigona*.[32] The minimization of the uncompensated resistance effect in the voltammetric measurements was achieved by the positive-feedback circuit of the potentiostat.

Photophysics. Absorption spectra were measured on a Varian Cary 5000 double-beam UV−vis−NIR spectrometer and baseline-corrected. Steady-state emission spectra were recorded on a Spex Fluorolog 1681 equipped with a 150 W xenon arc lamp, single excitation and emission monochromators, and a Hamamatsu R928 photomultiplier tube or a Horiba Jobin-Yvon IBH FL-322 Fluorolog 3 spectrometer equipped with a 450 W xenon arc lamp, double-grating excitation and emission monochromators (2.1 nm/mm dispersion; 1200 grooves/mm), and a Hamamatsu R928 photomultiplier tube or a TBX-4-X single-photon-counting detector. Emission and excitation spectra were corrected for source intensity (lamp and grating) and emission spectral response (detector and grating) by standard correction curves. Time-resolved measurements were performed using (i) a Coherent Infinity Nd:YAG-XPO laser (1 ns pulses of fwhm) and a Hamamatsu C5680-21 streak camera equipped with a Hamamatsu M5677 low-speed single-sweep unit and (ii) the time-correlated single-photon-counting option on the Fluorolog 3. NanoLEDs (295 or 402 nm; fwhm < 750 ps) with repetition rates between 10 kHz and 1 MHz were used to excite the sample. The excitation sources were mounted directly on the sample chamber at 90° to a double-grating emission monochromator (2.1 nm/mm dispersion; 1200 grooves/mm) and collected by a TBX-4-X single-photon-counting detector. The photons collected at the detector are correlated by a time-to-amplitude converter to the excitation pulse. Signals were collected using an IBH DataStation Hub photon-counting module, and data analysis was performed using the commercially available DAS6 software (Horiba Jobin Yvon IBH). The goodness of fit was assessed by minimizing the reduced χ^2 function and visual inspection of the weighted residuals. Luminescence quantum yields (Φ_{em}) were measured in optically dilute solutions (O.D. < 0.1 at excitation wavelength) and compared to reference emitters by the following equation:[33]

$$\Phi_x = \Phi_r \left[\frac{A_r(\lambda_r)}{A_x(\lambda_x)}\right]\left[\frac{I_r(\lambda_r)}{I_x(\lambda_x)}\right]\left[\frac{n_x^2}{n_r^2}\right]\left[\frac{D_x}{D_r}\right] \qquad (1)$$

where A is the absorbance at the excitation wavelength (λ), I is the intensity of the excitation light at the excitation wavelength (λ), n is the refractive index of the solvent, D is the integrated intensity of the luminescence, and Φ is the quantum yield. The subscripts r and x refer to the reference and sample, respectively. All quantum yields were performed at identical excitation wavelengths for the sample and reference, canceling the $I(\lambda_r)/I(\lambda_x)$ term in the equation. All iridium complexes were measured against quinine bisulfate in 1.0 N sulfuric acid as reference (1/4) 0.546. All solvents were spectrometric grade, and all solutions were filtered through a 0.2 μm syringe filter before measurement. Deaerated samples were prepared by the freeze−pump−thaw technique. Samples in the PMMA matrix were prepared by dissolving 5 mg of PMMA and 0.5 mg of the complex (10% in weight) in 1 mL of dichloromethane and then spin-coated onto glass substrates.

Computational Details. The optimization of the geometries and calculations of the molecular orbital energies were carried out by using the DFT method, with the B3LYP functional, the LANL2DZ relativistic effective core potential for iridium and bromine, and the 6-31G* basis set for carbon, hydrogen, and nitrogen. The absence of negative frequencies in the vibrational analysis was used as a parameter to confirm the reliability of the optimized geometries. The excited states of the complexes were calculated by using TD-DFT with the optimized ground-state geometries. All of the calculations were carried out with the *Gaussian 03* program.[34]

Ligand Syntheses. The ligands 2-(1*H*-tetrazol-5-yl)pyridine **PyTzH** and 2-(1*H*-tetrazol-5-yl)pyrazine **PzTzH** were prepared in good yields (80% for **PyTzH** and **PzTzH**) according to the first established method[35] involving 1,3 dipolar cycloaddition of the azide anion (N_3^-) on the appropriate aromatic nitriles, while the synthesis of the ligand 2-(1*H*-tetrazol-5-yl)-5-bromopyridine **BrPyTzH** (60% yield) was performed by following a slightly different procedure.[36] **PyTzH**: EI-MS (*m*/*z*) 146 ($M - H^+$, 100); ^{1}H NMR (DMSO-d_6, 400 MHz) 8.76 (d, H_6, $J = 4.6$ Hz), 8.19 (d, H_3, $J = 7.8$ Hz), 8.04 (t, H_4, $J = 7.8$ Hz), 7.59 (t, H_5, $J = 4.6$ Hz) ppm; ^{13}C NMR (DMSO-d_6, 100 MHz) 154.9 (C_t), 150.1 (C_6), 143.7 (C_2), 138.3 (C_4), 126.1 (C_5), 122.7 (C_3) ppm. **PzTzH**: EI-MS (*m*/*z*) 147 ($M - H^+$, 100); ^{1}H NMR (DMSO-d_6, 400 MHz) 9.37 (d, H_3, $J = 1.2$ Hz), 8.85 (m, 2H, H_5, H_6) ppm; ^{13}C NMR (DMSO-d_6, 100 MHz) 153.5 (C_t), 146.8 (C_5), 144.8 (C_6), 143.3 (C_3), 140 (C_2) ppm. **BrPyTzH**: EI-MS (*m*/*z*) 227 ($M^{\bullet+}$, 25), 169 ($M^+ - 2N_2$, 100); ^{1}H NMR (DMSO-d_6, 400 MHz) 8.92 (s, H_6), 8.31 (dd, H_4, $J = 8.4$ Hz, $J = 2.4$ Hz), 8.14 (d, H_3, $J = 8.4$ Hz) ppm; ^{13}C NMR (DMSO-d_6, 400 MHz) 154.5 (C_t), 151.0 (C_6), 142.5 (C_2), 140.9 (C_4), 124.2 (C_3), 122.6 (C_5) ppm.

(29) (a) La Pensée, A. A.; Bickley, J.; Higgins, S. J.; Marcaccio, M.; Paolucci, F.; Roffia, S.; Charnock, J. M. *J. Chem. Soc., Dalton Trans.* **2002**, 4095. (b) Cecchet, F.; Gioacchini, A. M.; Marcaccio, M.; Paolucci, F.; Roffia, S.; Alebbi, M.; Bignozzi, C. A. *J. Phys. Chem. B* **2002**, *106*, 3926.

(30) (a) Marcaccio, M.; Paolucci, F.; Paradisi, C.; Roffia, S.; Fontanesi, C.; Yellowlees, L. J.; Serroni, S.; Campagna, S.; Balzani, V. *J. Am. Chem. Soc.* **1999**, *121*, 10081. (b) Marcaccio, M.; Paolucci, F.; Paradisi, C.; Carano, M.; Roffia, S.; Fontanesi, C.; Yellowlees, L. J.; Serroni, S.; Campagna, S.; Balzani, V. *J. Electroanal. Chem.* **2002**, *532*, 99.

(31) Amatore, C.; Lefrou, C. *J. Electroanal. Chem.* **1992**, *324*, 33.

(32) Antigona developed by Dr. Loïc Mottier, University of Bologna, Bologna, Italy, 1999.

(33) Eaton, D. F. *Pure Appl. Chem.* **1988**, *60*, 1107.

General Procedure for the Preparation of Neutral Iridium(III)-Cyclometalated Complexes. A 100 mL round-bottomed flask protected from light was charged with 0.4 mmol (1 equiv) of $[(ppy)_2Ir(\mu\text{-}Cl)]_2$ and 1 mmol (2.5 equiv) of the appropriate tetrazole. The solid reactants were dissolved into a mixture of dichloromethane (10 mL) and ethanol (3 mL). The solution was stirred at room temperature for 4−6 h. Then, to the resulting yellow (in the case of **Ir(PyTz)** and **Ir(BrPyTz)**) or red-orange (for **IrPzTz**) mixture was added a 30 mL portion of hexanes, causing the formation of a precipitate, which was isolated by suction filtration. The resulting solid was washed with three 10 mL portions of hexanes and loaded onto an alumina-filled column. Elution with dichloromethane/acetone mixtures afforded the desired complexes **1**−**3** as the second fraction after small amounts of the starting $[(ppy)_2Ir(\mu\text{-}Cl)]_2$.

Ir(PyTz): 0.360 g (70%), yellow microcrystalline solid; ESI-MS (*m*/*z*) 669 ($M + Na^+$, 100); ^{1}H NMR (DMSO-d_6, 600 MHz) 8.34 (d, H_3, $J_{HH} = 8.4$ Hz), 8.17 (d, 2H, $J = 7.8$ Hz), 8.12 (t, H_4, $J = 7.2$ Hz), 7.87−7.84 (m, 3H), 7.80 (d, 1H, $J = 7.2$ Hz), 7.68 (d, H_6, $J = 4.8$ Hz), 7.55 (d, 1H, $J = 5.4$ Hz), 7.48 (t, H_5, J= 7.2 Hz), 7.42 (d, 1H, $J = 5.4$ Hz), 7.15 (t, 1H, $J = 7.2$ Hz), 7.11 (d, 1H, $J = 7.2$ Hz), 6.97 (t, 1H, $J = 7.2$ Hz), 6.91−6.85 (m, 2H), 6.76 (t, 1H, $J = 7.2$ Hz), 6.22 (d, 1H, $J = 6.6$ Hz), 6.17 (d, 1H, $J = 7.2$ Hz) ppm; ^{13}C NMR (DMSO-d_6, 100 MHz) ppy's 167.4, 167.2, 151.8, 148.9, 148.7, 147.6, 144.4, 144.1, 138.5, 138.1, 131.5, 131.4, 130.1, 129.2, 124.9, 124.4, 123.6, 123.4, 122.0, 121.3, 119.7, 119.5; tetrazolate ligand **PyTz** 163.6 (C_t), 149.6 (C_6), 148.2 (C_2), 140.0 (C_4), 126.8 (C_5), 122.5 (C_3) ppm. Suitable crystals for X-ray diffraction experiments were obtained by the slow diffusion of diethyl ether into a dichloromethane solution of the complex **Ir(PyTz)**, which crystallized as **[Ir(PyTz)]·CH_2Cl_2**. Anal. Calcd for $C_{29}H_{22}N_7Cl_2Ir$ (731.09): C, 47.60; H, 3.03; N, 13.41. Found: C, 47.50; H, 3.05; N, 13.35.

Ir(PzTz): 0.280 g (54%), red microcrystalline solid; ESI-MS (*m*/*z*) 670 ($[M + Na]^+$, 100); ^{1}H NMR (CD_2Cl_2, 600 MHz) 9.62 (d, H_3, $J = 1.2$ Hz), 8.49 (d, H_5, $J = 3$ Hz), 7.92 (d, 1H, $J = 8.4$ Hz), 7.89 (d, 1H, $J = 7.8$ Hz), 7.78 (dd, H_6, $J = 3$ Hz, $J = 1.2$ Hz), 7.74−7.7 (m, 4H), 7.57 (d, 1H, $J = 6.6$ Hz), 7.46 (d, 1H, $J = 6.6$ Hz), 7.05 (t, 1H, $J = 7.8$ Hz), 7.01 (t, 1H, $J = 7.8$ Hz), 6.95−6.87 (m, 4H), 6.39 (d, 1H, $J = 7.2$ Hz), 6.31 (d, 1H, $J = 7.2$ Hz) ppm; ^{13}C NMR (CD_2Cl_2, 100 MHz) ppy's 168.2, 167.9, 150.5, 150.2, 148.6, 145.0, 144.8, 143.9, 138.2, 137.9, 132.3, 131.9, 130.7, 130.1, 125.0, 124.6, 123.5, 123.0, 122.3, 119.8, 119.6 ppm; tetrazolate ligand **PzTz** 162.2 (C_t), 148.2 (C_5), 147.3 (C_3), 147.0 (C_6), 144.6 (C_2) ppm. Suitable crystals for X-ray diffraction experiments were obtained by the slow diffusion of diethyl ether into a dichloromethane solution of the complex **Ir(PzTz)**. Anal. Calcd for $C_{27}H_{19}N_8Ir$ (648.14): C, 49.99; H, 2.95; N, 17.28. Found: C, 50.01; H, 2.98; N, 17.34. **Ir(BrPyTz)**: 0.340 g (59%), yellow-red microcrystalline solid; ESI-MS (*m*/*z*) 748 ($[M + Na]^+$, 100); ^{1}H NMR (CD_2Cl_2, 600 MHz) 9.30 (d, H_3, $J = 9$ Hz), 8.07 (d, H_4, $J = 8.4$ Hz), 7.90 (t, 2H, $J = 7.8$ Hz), 7.82 (s, H_6), 7.73−7.68 (m, 4H), 7.59 (d, 1H, $J = 7.2$ Hz), 7.52 (d, 1H, $J = 7.2$ Hz), 7.05 (t, 1H, $J = 7.2$ Hz), 6.99 (t, 1H, $J = 7.2$ Hz), 6.95−6.91 (m, 3H), 6.86 (t, 1H, $J = 7.2$ Hz), 6.37 (d, 1H, $J = 7.8$ Hz), 6.30 (d, 1H, $J = 7.8$ Hz) ppm; ^{13}C NMR (CD_2Cl_2, 150.8 MHz) ppy's 168.3, 168.1, 150.2, 150.1, 148.8, 146.7, 144.8, 144.1, 138.0, 137.7, 132.3, 132.0, 130.7, 130.0, 125.0, 124.6, 123.3, 122.9, 122.7, 122.1, 119.7, 119.6 ppm; tetrazolate ligand **BrPyTz** 163.5 (C_t), 151.4 (C_2), 151.2 (C_6), 141.9 (C_4), 123.7 (C_3), 121.9 (C_5) ppm. Suitable crystals for X-ray diffraction experiments were obtained by the slow diffusion of diethyl ether into a dichloromethane solution of the complex **Ir(BrPyTz)**. Anal. Calcd for $C_{28}H_{19}N_7BrIr$ (725.05): C, 46.34; H, 2.64; N, 13.52. Found: C, 46.30; H, 2.68; N, 13.60.

Procedure for the Methylation of Ir(PyTz). Synthesis of [Ir(PyTzMe)][PF_6]. A 0.100 g (0.15 mmol) quantity of the starting complex **Ir(PyTz)** was dissolved in dichloromethane (10 mL), and the resulting yellow mixture was cooled to −50 °C. A slight excess of methyl triflate (1.1 mL, 0.150 M in dichloromethane, 0.165 mmol) was successively added dropwise to the vigorously stirred solution. After 30 min at −50 °C, the canary-yellow mixture was allowed to warm to room temperature and stirred for an additional 6 h. Evaporation of the solvent afforded a yellow oily residue, which was dissolved into a minimal amount of ACN to which was added 10 mL of an aqueous solution containing ca. 0.5 g of NH_4PF_6. The resulting mixture was extracted with dichloromethane (3 × 20 mL) until the aqueous phase became colorless. The organic layers were dried over $MgSO_4$, and the solvent was removed in vacuo, affording a crude product, which was purified by alumina-filled column chromatography with ACN/toluene mixtures as the eluent. The saline compound **[Ir(PyTzMe)][PF_6]** (0.110 g, 88%) was recovered as the second yellow fraction after a small amount of the starting **Ir(PyTz)**: ESI-MS (*m*/*z*) 662 (M^+, 100); ^{1}H NMR (CD_3CN, 600 MHz) 8.40 (d, H_3, $J = 7.6$ Hz), 8.16 (t, H_4, $J = 8$ Hz), 8.05 (d, 2H, $J = 8$ Hz), 7.90 (d, H_6, $J = 4.8$ Hz), 7.89−7.83 (m, 2H), 7.78 (d, 1H, $J = 8$ Hz), 7.73 (d, 1H, $J = 8$ Hz), 7.61 (d, 1H, $J = 5.6$ Hz), 7.56 (t, H_5, $J = 7.2$ Hz), 7.1−7.03 (m, 3H), 6.99−6.89 (m, 2H), 6.84 (t, 1H, $J = 8$ Hz), 6.25 (d, 2H, $J = 7.6$ Hz), 4.42 (s, 3H, Me) ppm; ^{13}C NMR (CD_3CN, 100 MHz) ppy's 168.3, 167.9, 151.1, 150.6, 148.5, 145.4, 145.3, 139.8, 139.7, 132.9, 132.3, 131.3, 130.7, 125.9, 125.4, 124.6, 124.5, 123.9, 123.5, 120.9, 120.7 ppm; tetrazolate ligand**[PyTzMe]** 167.7 (C_t), 152.2 (C_6), 145.2 (C_2), 141.3 (C_4), 130.5 (C_5), 125.5 (C_3), 42.7 (Me) ppm. Suitable crystals for X-ray diffraction experiments were obtained by the slow diffusion of diethyl ether into a dichloromethane solution of the complex **[Ir(PyTzMe)][PF_6]**, which crystallized as **[Ir(PyTzMe)][PF_6]·CH_2Cl_2**. Anal. Calcd for $C_{30}H_{25}N_7Cl_2IrF_6P$ (891.08): C, 40.40; H, 2.83; N, 11.00. Found: C, 40.44; H, 2.78; N, 10.92.

Homocoupling Reaction of Ir(BrPyTz). Synthesis of [Ir(PyTz)]$_2$. This reaction was performed by addressing some small modification to a reported procedure.[37] A 0.100 g (0.14 mmol) aliquot of **Ir(BrPyTz)** and 0.02 g of *cis*-$Pd(PhCN)_2Cl_2$ (PhCN is benzonitrile) were charged into a 100 mL two-necked, round-bottomed flask. The solid reactants were dissolved into 5 mL of freshly distilled DMF, and an excess (1 mL) of triethylamine was added to the yellow solution. The temperature was then raised to

(34) Frisch, M. J.; Trucks, G. W.; Schlegel, H. B.; Scuseria, G. E.; Robb, M. A.; Cheeseman, J. R.; Montgomery, J. A., Jr.; Vreven, T.; Kudin, K. N.; Burant, J. C.; Millam, J. M.; Iyengar, S. S.; Tomasi, J.; Barone, V.; Mennucci, B.; Cossi, M.; Scalmani, G.; Rega, N.; Petersson, G. A.; Nakatsuji, H.; Hada, M.; Ehara, M.; Toyota, K.; Fukuda, R.; Hasegawa, J.; Ishida, M.; Nakajima, T.; Honda, Y.; Kitao, O.; Nakai, H.; Klene, M.; Li, X.; Knox, J. E.; Hratchian, H. P.; Cross, J. B.; Bakken, V.; Adamo, C.; Jaramillo, J.; Gomperts, R.; Stratmann, R. E.; Yazyev, O.; Austin, A. J.; Cammi, R.; Pomelli, C.; Ochterski, J. W.; Ayala, P. Y.; Morokuma, K.; Voth, G. A.; Salvador, P.; Dannenberg, J. J.; Zakrzewski, V. G.; Dapprich, S.; Daniels, A. D.; Strain, M. C.; Farkas, O.; Malick, D. K.; Rabuck, A. D.; Raghavachari, K.; Foresman, J. B.; Ortiz, J. V.; Cui, Q.; Baboul, A. G.; Clifford, S.; Cioslowski, J.; Stefanov, B. B.; Liu, G.; Liashenko, A.; Piskorz, P.; Komaromi, I.; Martin, R. L.; Fox, D. J.; Keith, T.; Al-Laham, M. A.; Peng, C. Y.; Nanayakkara, A.; Challacombe, M.; Gill, P. M. W.; Johnson, B.; Chen, W.; Wong, M. W.; Gonzalez, C.; Pople, J. A. *Gaussian 03, revision C.02*; Gaussian, Inc.: Wallingford, CT, 2004.
(35) Finnegan, W. G.; Henry, R. A.; Lofquist, R. *J. Am. Chem. Soc.* **1958**, *80*, 3909.
(36) Jo, Y. W.; Im, W. B.; Rhee, J. K.; Shim, M. J.; Kim, W. B.; Choi, E. C. *Bioorg. Med. Chem.* **2004**, *12*, 5909.
(37) Kuroboshi, M.; Waki, Y.; Tanaka, H. *J. Org. Chem.* **2003**, *68*, 3938.

Table 7. Crystal Data and Experimental Details for **Ir(PyTz)·CH_2Cl_2**, **Ir(PzTz)**, **Ir(BrPyTz)**, and **[Ir(PyTzMe)][PF_6]CH_2Cl_2**

complex	**Ir(PyTz)·CH_2Cl_2**	**Ir(PzTz)**	**Ir(BrPyTz)**	**[Ir(PyTzMe)][PF_6]·CH_2Cl_2**
empirical formula	$C_{29}H_{22}Cl_2IrN_7$	$C_{27}H_{19}IrN_8$	$C_{28}H_{19}BrIrN_7$	$C_{30}H_{25}Cl_2F_6IrN_7P$
fw	731.64	647.70	725.61	891.64
T, K	294(2)	295(2)	293(2)	293(2)
λ, Å	0.710 73	0.710 73	0.710 73	0.0710 73
cryst syst	orthorhombic	monoclinic	monoclinic	monoclinic
space group	$P2_12_12_1$	$P2_1/n$	$P2_1/c$	$P2_1/c$
a, Å	9.7337(7)	8.9141(3)	16.631(3)	15.1265(9)
b, Å	11.8884(9)	21.8339(8)	9.1592(18)	13.3577(8)
c, Å	23.3608(17)	12.0285(4)	18.092(4)	17.5960(10)
β, deg	90	97.5320(10)	114.74(3)	111.0650(10)
cell volume, $Å^3$	2703.3(3)	2320.90(14)	2503.0(9)	3317.8(3)
Z	4	4	4	4
D_c, g cm^{-3}	1.798	1.854	1.926	1.785
μ, mm^{-1}	5.170	5.787	6.963	4.301
$F(000)$	1424	1256	1392	1736
cryst size, mm	0.21 × 0.16 × 0.12	0.20 × 0.15 × 0.12	0.22 × 0.21 × 0.14	0.24 × 0.21 × 0.15
θ limits, deg	1.74−28.00	1.87−27.00	1.24−25.03	1.44−27.10
reflns collected	23 576	25 651	23 545	36 471
indep reflns	6391 [R_{int} = 0.0542]	5059 [R_{int} = 0.0362]	4425 [R_{int} = 0.0457]	7315 [R_{int} = 0.0263]
data/restraints/parameters	6391/0/352	5059/0/325	4425/163/335	7315/188/423
GOF on F^2	1.081	1.024	1.103	1.038
R1 [$I > 2\sigma(I)$]	0.0403	0.0226	0.0673	0.0335
wR2 (all data)	0.0754	0.0516	0.2179	0.1004
largest diff peak and hole, e $Å^{-3}$	0.770/−1.499	0.778/−0.413	3.710/−2.210	1.553/−1.552

50 °C, and the mixture was vigorously stirred for 5 h, during which time the color turned from yellow to brown. After cooling to room temperature, the mixture was poured into 100 mL of ice/water and extracted with three 20 mL portions of dichloromethane. The organic layers were then combined, washed with 50 mL of aqueous $NaHCO_3$, and dried over $MgSO_4$. Then, the solvent was removed under reduced pressure, affording a dark-yellow crude product, which was purified by alumina-filled column chromatography. Elution with a dichloromethane/acetone (1:1.5, v/v) mixture afforded the target dinuclear species **[Ir(PyTz)]$_2$**(0.070 g, yellow powder, 77%): ESI-MS (*m*/*z*) 1315 (M + Na^+, 100); ^{1}H NMR (CD_2Cl_2, 600 MHz) 8.38 (d, 2H$_3$, J = 8.4 Hz), 7.93 (t, 2H, J = 7.2 Hz), 7.91 (t, 2H$_4$, J = 8.4 Hz), 7.87 (d, 2H$_6$, J = 4.8 Hz), 7.81 (d, 2H, J = 5.4 Hz), 7.71−7.68 (m, 8H), 7.61 (d, 2H, J = 5.4 Hz), 7.49 (d, 2H, J = 5.4 Hz), 7.22 (t, 2H, J = 5.4 Hz), 7.04−6.98 (m, 4H), 6.93−6.84 (m, 6H), 6.39 (d, 2H, J = 7.2 Hz), 6.33 (d, 2H, J = 7.2 Hz) ppm; ^{13}C NMR (CD_2Cl_2, 100 MHz) ppy's 168.5, 168.1, 150.4, 150.0, 148.8, 147.8, 144.8, 144.2, 137.8, 137.5, 132.3, 132.1, 130.5, 129.9, 126.0, 124.8, 124.6, 123.2, 122.9, 122.4, 122.0, 119.6, 119.4; tetrazolate ligand **[PyTz]$_2$** 164.2 (C_t), 152.3 (C_2), 150.1 (C_6), 139.1 (C_4), 126.0 (C_5), 122.6 (C_3) ppm. Anal. Calcd for $C_{56}H_{38}N_{14}Ir_2$ (1292.27): C, 52.00; H, 2.96; N, 15.17. Found: C, 52.10; H, 3.00; N, 15.21.

X-ray Crystallography. Crystal data and collection details for **Ir(PyTz)·CH_2Cl_2**, **Ir(PzTz)**, **Ir(BrPyTz)**, and **[Ir(PyTzMe)][PF_6]·CH_2Cl_2** are reported in Table 7. The diffraction experiments were carried out on a Bruker SMART 2000 diffractometer equipped with a CCD detector using Mo Kα radiation. Data were corrected for Lorentz polarization and absorption effects (empirical absorption correction *SADABS*).[38] Structures were solved by direct methods and refined by full-matrix least squares based on all data using F^2.[39] Hydrogen atoms were fixed at calculated positions and refined by a riding model. All non-hydrogen atoms were refined with anisotropic displacement parameters, unless otherwise stated. The CH_2Cl_2 molecule in **[Ir(PyTzMe)][PF_6]·CH_2Cl_2** is disordered. Disordered atomic positions were split and refined isotropically using similar distance and similar U restraints and one occupancy parameter per disordered group. The crystals of **Ir(BrPyTz)** are nonmerohedrally twinned. The program *CELL_NOW* was used for indexing and determination of the twinning matrix.[40] Data were integrated by *SAINT* using the main domain.[41] The TWIN routine of *SHELX97* was used during the refinement with the appropriate twin matrix (1 0 0.769 0 −1 0 0 0 −1), giving a final BASF factor of 0.06575.

Acknowledgment. The authors thank the Italian Ministero dell'Istruzione, Università e Ricerca (MIUR), for financial support. The University of Bologna, the Faculty of Industrial Chemistry of the University of Bologna (postgraduate grant to S.C.), and the Alexander von Humboldt foundation (financial support to R.Q.A.), and LATEMAR (centre of excellence financed by MIUR) are gratefully acknowledged.

Supporting Information Available: NMR (^{1}H and ^{13}C) spectra of all compounds, absorption and emission spectra recorded at 77 K and in a PMMA matrix, a table with some selected bond distances, a plot of the frontier molecular orbitals of **[Ir(PyTzMe)]$^+$** in its one-electron-reduced state, X-ray crystallographic files in CIF format for the crystal structure determinations of complexes **Ir(PyTz)**, **Ir(PzTz)**, **Ir(BrPyTz)**, and **[Ir(PyTzMe)]$^+$**. This material is available free of charge via the Internet at http://pubs.acs.org.

IC801157K

(38) Sheldrick, G. M. *SADABS, Program for empirical absorption correction*; University of Göttingen: Göttingen, Germany, 1996.
(39) Sheldrick, G. M. *SHELX97, Program for crystal structure determination*; University of Göttingen: Göttingen, Germany, 1997.
(40) Sheldrick, G. M. *CELL_NOW, Program for unit cell determination*; University of Göttingen: Göttingen, Germany, 2005.
(41) *APEX2 User Manual*; Bruker AXS Inc.: Madison, WI, 2005.